MULTI-PHYSICS MODELLING AND SIMULATION OF A DISTRIBUTED ELECTRIC PROPULSION SYSTEM FOR HELICOPTER ANTI-TORQUE

Massimo Brunetti[1], Andrea Nesci[2], Luca Feltrin[3], Daniele Michieletto[3], Loris Vianello[3] and Nicola Bianchi[3]

[1] Research and Innovation Office, Leonardo Helicopters Division, Leonardo S.p.A.
massimo.brunetti@leonardo.com
[2] Chief Technology and Innovation Office, Leonardo Labs, Leonardo S.p.A.
andrea.nesci.ext@leonardo.com
[3] Department of Industrial Engineering, University of Padova, Padova, Italy
nicola.bianchi@unipd.it

ABSTRACT

The flexibility offered by Distributed Electric Propulsion (DEP) has triggered in the recent years a variety of new aircraft demonstrators, showing a way to improve the overall efficiency, capabilities and robustness of the future air-vehicles [1]. In comparison, the conventional helicopter tail rotor, with its vulnerable and complex installation, looks like an example of system application ready to take advantage of DEP, both in terms of redundancy and simplification of the flight control chain. This paper investigates the behavior of a distributed electric anti-torque system, starting from a reference usage spectrum and a fixed-pitch/variable-speed rotor design. The goal is to optimize the key electrical components for steady state operation and to verify the dynamic behavior of the system in healthy as well as in degraded conditions. Following an introduction to the safety requirements and the electrical technology state-of-the-art, all the main components are modelled and combined into a single dynamic network. Simulation results from different testing scenarios are then reviewed (in the mechanical, thermal and electrical domain) to show compliance with the minimum acceptance criteria. Finally, the article discusses the advantages and disadvantages of a distributed versus concentrated electrical solution.

NOMENCLATURE

Symbols

α	Convection coefficient	W/m^2/K
Θ	Overtemperature	K
κ	Thermal conductivity	W/m/K
λ	Failure rate	failures/h
μ	Advance ratio	-
ρ	Density	kg/m^3
τ	Torque	Nm
ω	Rotational speed	rad/s
A	Area	m^2
c	Specific heat	J/kg/K
C	Thermal capacity	J/K
C_{k+1}^n	n elements, $k+1$-combinations	-
C_P	Power coefficient	-
C_T	Thrust coefficient	-
I	Current	A
F	Probability of failure	-
l	Length	m
J	Moment of inertia	kg m^2
k	Number of failures	-
N	Number of cells	-
n	Number of motor drives	-
P	Power	W
p.u.	per unit	-
$\dot{Q}$	Heat transfer rate	W
Q_{cell}	Cell capacity	Ah
r	Tail rotor radius	m
R	Resistance (electric)	Ω
	Resistance (thermal)	K/W
T	Thrust	N
t	Time	s
U	Voltage	V
v	Speed	m/s
V	Volume	m^3
x	Overload (torque)	-

Subscripts

em	Electromagnetic
mr	Main Rotor
oc	Open circuit
rot	Rotor
tr	Tail Rotor

1 INTRODUCTION

Figure 1: Sikorsky R-4 helicopter.

Since the introduction of the R-4 by Igor Sikorsky, in 1942, single main rotor helicopters have widespread and become the most popular configuration in the world. In order to counteract the main rotor yawing moment, this configuration requires an anti-torque system. Which is typically comprehensive of a secondary rotor, positioned at the end of the tail boom and connected to the engine, via a number of shafts and gearboxes. Although refined over the years, this solution is still sub-optimal (as tail rotor is forced to revolve at a constant speed, regardless of the flight condition) and cause of concerns (due to the exposure and complexity of the tail rotor installation) [2]. Previous research initiatives carried out by Leonardo Helicopters have tried to enhance the system efficiency and reliability by direct electrification of the tail rotor drive [3]. This could also mitigate the noise footprint and the maintenance labour, thanks to a reduced number of system parts and the possibility to slow down the tail rotor, in cruise. However, waiting for major technology breakthroughs, a single electrical machine Form Fit Function (FFF) to a conventional helicopter tail gearbox remains quite heavy [4].

As an alternative, Distributed Electric Propulsion (DEP) can bring in an intrinsic redundancy at system level, synthesizing the required thrust vector by superposition of multiple tail rotor effects. Beyond eliminating any single point of failure, this solution can enable a streamline, sheltered arrangement of the rotors within the tail structure (Fig. 2). Moreover, since tail rotors would operate at low advance ratios, the Electronic Speed Control (ESC) could replace the mechanical pitch control. Which in return could simplify the rotor design, lower the inertia and improve the system response. For a maximum blade tip speed, several smaller tail rotors would also spin at a higher angular speed. Which considered the dependency of the electrical machines mass on torque could reduce the system weight.

Starting from a reference helicopter anti-torque usage spectrum and a datum tail rotor design, this paper investigates the behaviour of the system for an optimal sizing of its key electrical components, based on a multi-physics modelling and simulation approach. For instance, tail rotor thrust is mapped into torque, through the characteristic aerodynamic coefficients and disc area. Tail motor power ratings are computed accounting for both the magnetic and the thermal limitations. Generator voltage output is evaluated as a function of the load current and the input shaft speed. The power that a battery pack can release is affected by its internal State-of-Charge (SoC).

2 SYSTEM ARCHITECTURE

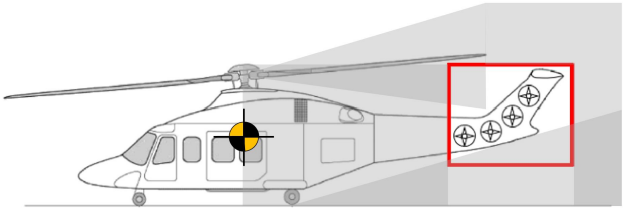

Figure 2: Leonardo anti-torque concept.

When dealing with DEP, the definition of the number, size and position of the rotors is a complex task depending on multiple trade-off. While structural optimization would require more concentrated configurations, electric power-on-weight and aerodynamic thrust-on-power tend to improve by the opposite [5]. In the case of a helicopter anti-torque system, a number of additional constraints limit the space of the possible solutions to the area comprised between the upper main rotor flapping, the lower ground clearance, the maximum tail dimension and the minimum distance from the aircraft Center of Gravity (CoG). The partitioning of this area requires relatively small tail rotors, hence relatively compact and light tail motors. Such to avoid the risk of rotor blockage and nose *pitch-up*; efficient enough to go with the air-cooling offered by the rotors.

Table 1: PMSM performance (air-cooled).

Efficiency (including PE)	$\geq 90\%$
Overload (torque)	up to 200%
Failure rate	$\leq 10^{-4}$

Table 2: Required motor torque as a function of the number of failures and motor-drives.

Torque [p.u] HOGE		N. of motor-drives (n) 1	2	3	4	5	6	7	8	Probability $(k+1)$
N. of failures (k)	0	1.5	1.5	1.5	1.5	1.5	1.5	1.5	1.5	$\simeq n \cdot 10^{-4}$
	1	–	3	2.25	2	1.87	1.8	1.75	1.7	$\simeq \frac{n!}{2(n-2)!} \cdot 10^{-8}$
	2	–	–	4.5	3	2.5	2.25	2.1	2	$\simeq \frac{n!}{6(n-3)!} \cdot 10^{-12}$
	3	–	–	–	6	3.75	3	2.65	2.4	$\simeq \frac{n!}{24(n-4)!} \cdot 10^{-16}$

All these requirements are essentially met by Permanent Magnet Synchronous Machines (PMSMs). Readily available on the market with the performance summarized in Tab. 1, this technology can be easily adapted to different vehicle installations and it has quickly become the de-facto solution for electric Vertical Take-Off and Landing (eVTOL) applications. Even compatible with embedded Power Electronics (PE), PMSMs can add a further level of redundancy at component level and contribute to make the anti-torque system fail-operative or at least fail-soft [6].

As shown in the next section, the peak of the load is reached in Hovering Out of Ground Effect (HOGE). A flight phase which usually lasts no more than few minutes but that for safety reasons must be guaranteed for at least some seconds. For instance, to accomplish a vertical landing on an oil rig, or to quit a rescue hoist operation. Then, supposing to adopt the existing technology and to make the loss of the required functionality "extremely improbable" (i.e. with a probability equal/less than 10^{-9}, consistently with the regulatory framework [7]), the following constraints apply:*

$$(1) \qquad \begin{cases} \frac{n}{n-k}\, x \leq 2 \\ \\ C_{k+1}^{n}\, \lambda^{k+1} \leq 10^{-9} \end{cases}$$

Where, n is the number of motor-drives, k the number of failures, x the overload in HOGE, λ the PMSM failure rate and C_{k+1}^{n} is the $k+1$-combinations of the n elements, given by the binomial coefficient:

$$(2) \qquad C_{k+1}^{n} = \binom{n}{k+1} = \frac{n!}{(k+1)!\,(n-k-1)!}$$

*because a helicopter mission is considered, the characteristic time is close to unity ($t \simeq 1$ h) and the probability of failure $F(t)$ can be approximated by the failure rate:

$$F(t) = \int_0^t \lambda\, e^{-\lambda\tau} d\tau = 1 - e^{-\lambda t} \simeq 1 - (1 - \lambda t) \simeq \lambda$$

Note that design point in HOGE is somewhat arbitrary and that the higher the overload, the lighter the motor and the shorter the endurance. In particular, for $x = 1.5$ (i.e. the mid-point between the peak and the nominal torque p.u.), the exploration of the (n, k) design space shown in Tab. 2 leads to a minimum of eight motor-drives, which can tolerate up to 2 failures, being the third extremely improbable. Therefore, the system configuration depicted in Fig. 2, having four tail rotors driven by as many PMSMs (equipped with a Dual Three-Phase winding [8]) can be considered acceptable.

On the other hand, any electrical machine can either operate as a motor or a generator. The use of a PMSM unit integrated with a turbo-shaft and operating at high rpm can thus complete the system and make the generation equally light and compact than the actuation. Since electrical power would flow almost uninterruptedly from the generator to the motors, the resulting architecture may be regarded as *turbo-electric* [9]. However, it is anticipated that the system behavior benefited by the presence of a battery pack. This component, primarily introduced to back up the generator in case of engine failure, was indeed found to be useful also to shave the peaks of the load and to absorb the current regenerated by the motors, during active rotor braking (Fig. 3).

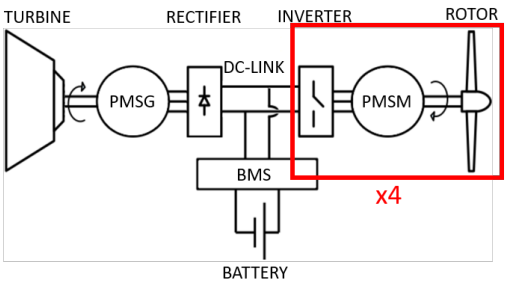

Figure 3: System block diagram (notional).

3 SUBSYSTEM MODELS

The models presented in this section express the capability of each drive-train component, as a function of its physical characteristics and the internal status. These models have been also exploited for a preliminary optimization of the motors and the battery, separately, prior to their combination into a single dynamic network.

3.1 Rotor model

In the proposed system configuration, the anti-torque effect is controlled by adjusting the tail rotor angular speed. Therefore, in order to simulate the system behavior, it is necessary to find the mathematical relationship existing between the two.

This can be done starting from the analysis of the main rotor power profile, as a function of the helicopter forward speed or *advance ratio*, Fig. 4. Such a profile has two peaks, respectively at zero and at high advance ratios, which stem from multiple power contributions including the induced power, profile power and parasitic power of the rotor. Since a higher absorbed power involves a higher yawing moment impinging on the fuselage and since the tail fin is essentially ineffective at low forward speed, the most demanding flight condition for the anti-torque system is in hover. In which case the whole yawing moment is counteracted by accelerating the rotors (and the air) to the maximum speed. So that the maximum rotor thrust and rotor torque is produced.

In particular, in order to achieve a mechanical balance, the four tail rotors must provide an anti-torque effect which is equal to the yawing moment and that assuming the same thrust for each unit can be expressed as:

$$\tau_{mr} = T_{tr}\,(l_1 + l_2 + l_3 + l_4) \tag{3}$$

Where $l_{1,2,3,4}$ are the distances between the tail rotor hubs and the helicopter CoG. Eq. 3 allows to compute the individual tail rotor thrust in HOGE, or in any other flight condition, supposing that the lateral stabilization effect provided by the tail fin is negligible (or already deducted from the main rotor yawing moment). The individual tail rotor thrust can be then traced back to the angular rotor speed, ω_{tr}, via the tail rotor thrust coefficient, C_T, using the momentum theory [10]–[12]:

$$T_{tr} = \rho_{air}\,A\,(\omega_{tr}\,r)^2\,C_T \tag{4}$$

Where A is the tail rotor disc area, r its radius and ρ_{air} is the air density as function of altitude.

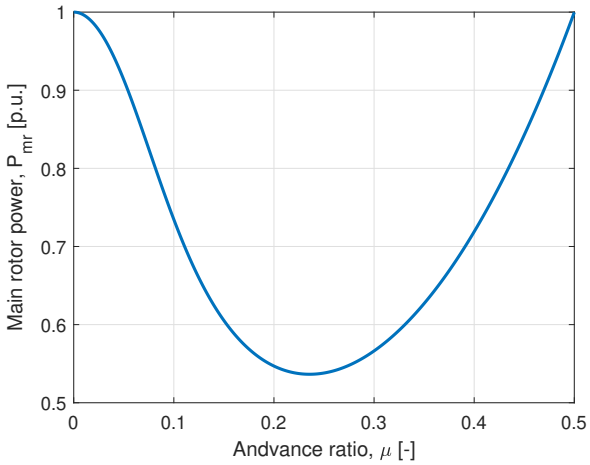

Figure 4: Main rotor power vs helicopter advance ratio.

In a similar manner, the individual tail rotor power can be expressed through the power coefficient, C_P:

$$P_{tr} = \rho_{air}\,A\,\omega_{tr}^3\,r^3\,C_P \tag{5}$$

In general, both C_T and C_P depend on the considered flight condition but it is worth noting that combining Eq. (4) with (5) it is possible to obtain the following relationship which is always valid:

$$\tau_{tr} = T_{tr}\left(\frac{C_P}{C_T}\right) r \tag{6}$$

Hence, for a certain fixed-pitch rotor geometry (r, C_P, C_T = constant) the rotor/motor torque is directly proportional to the required thrust, as a function of the main rotor yawing moment and tail rotor hub position. This allows to define the set of steady-state operating points summarized in Tab. 3 and depicted in Fig. 5. Which represents the map of the required anti-torque effect, for the different flight conditions, into a torque-speed reference frame.

Table 3: Steady-state operating points.

Helicopter manoeuvre	**Time** [min]	**4 TR Operative** **Torque** [p.u.]	**Speed** [p.u.]	**3 TR Operative** **Torque** [p.u.]	**Speed** [p.u.]
Take-off	2	1.33	0.81	1.77	0.94
Climb	5	0.62	0.57	0.85	0.65
Cruise	10	0.35	0.42	0.46	0.48
HOGE	5	1.5	0.87	2	1
Cruise	10	0.35	0.42	0.46	0.48
Descent	5	0.24	0.35	0.32	0.4
Landing	2	1.23	0.78	1.64	0.91

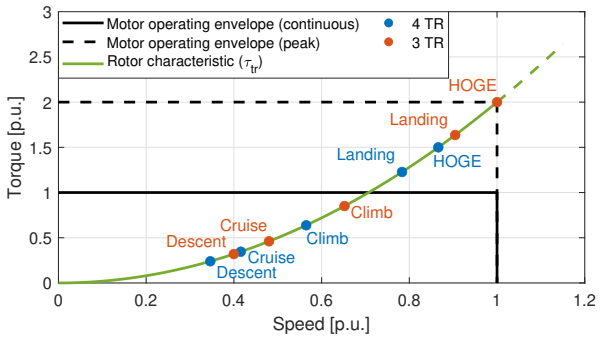

Figure 5: Motor operating points on rotor characteristic.

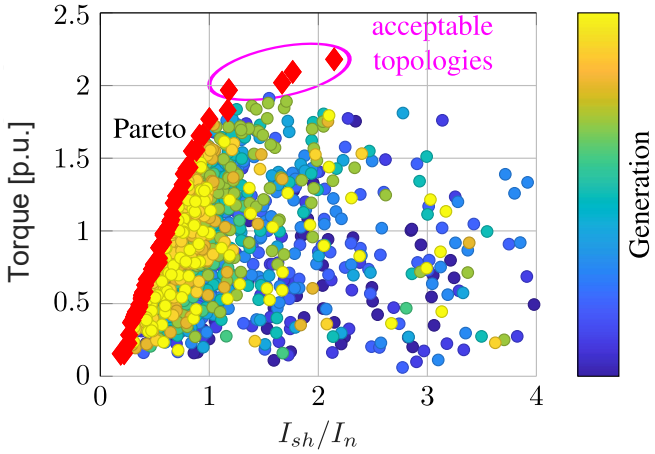

Figure 6: Electric motor genetic optimization.

3.2 Motor model

The feasibility of the proposed architecture is based on the assumption that four tail motors built in the PMSM technology with a Dual Three-Phase winding are equivalent to eight independent motor-drives. Consistently, the supposed fault tolerance was modeled and verified against the target operating conditions.

Dual Three-Phase winding allows for a simple control strategy since the stator winding is split into two subsystems supplied by two separate inverters. In principle, in the event of a fault of one winding, this is disconnected and the machine can continue to operate by means of the other. In practice, in case of a short-circuit, the induced current may be so high to exceed the demagnetization or thermal limits of the healthy machine parts [13]. The first step to achieve a *true* fault tolerant design is to thus map the whole set of system operating conditions into the motor characteristic torque-speed reference frame (see Tab. 3).

These conditions should be sustained in the worst foreseeable scenario, that from an electrical perspective, corresponds to a complete motor loss. If so, not only the remaining rotors/motors must provide the missing thrust/torque contribution, but they have also to operate at a higher disc-loading/angular-speed. Which results in a significant absorbed power increment (and efficiency degradation). For this reason, the HOGE with three-on-four tail rotors can be considered as the motor *sizing* condition.

The motor design was then optimized through a genetic algorithm, setting as objectives: **(i)** the maximization of the electromagnetic torque, **(ii)** the minimization of the ratio between the short circuit and the nominal current. The algorithm was developed to explore the key geometrical parameters of the motor such the slot dimension, the magnet size, the air-gap etc., and evaluate for each combination a global figure of cost. In particular, some of the parameters were set from the beginning equal to a specific value, due to the constraints imposed by a realistic installation. For instance, this happened for the stack length and the case diameter, both related to the compatibility of the motor with the available tail volume and air-cooling mechanism, through the slot current density. Fig. 6 shows the evolution of the geometrical parameters in the plane of the optimization objectives, where the short-to-nominal current ratio is on the x axis and the electromagnetic torque is on the y axis. The red diamond markers highlight the Pareto front of the cost function.

Once the key geometrical parameters were optimized, the Finite Element Method (FEM) was used to estimate some additional electrical parameters, such the permanent magnet flux linkage Λ_m, the stator phase resistance R_s and the stator synchronous inductance L_s. These parameters define the motor equivalent circuit model in the d-q reference frame [14], and along with the following expression of the electromagnetic torque (valid for each of the two winding subsystems) allow to capture the motor electromechanical dynamics:

$$\tau_{em} = \frac{3}{2} p \Lambda_m I_q \tag{7}$$

Where p is the number of pole pairs and I_q is the stator q-axis current. While I_d is the stator d-axis current, set to zero in the absence of flux weakening. So that in Fig. 7, relevant to the adopted Field Oriented Control (FOC) scheme, the motor torque is adjusted through I_q only.

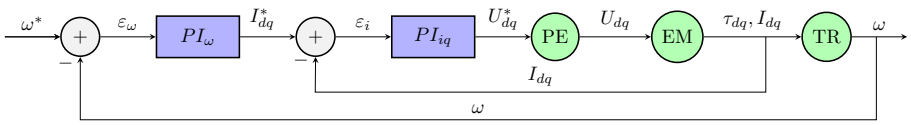

Figure 7: Adopted motor control scheme (FOC).

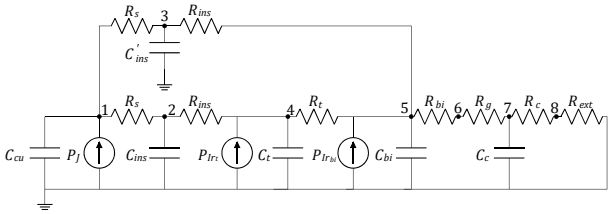

Figure 8: Motor lumped parameter thermal network.

In addition, a lumped parameter thermal network was developed for the purpose to monitor the temperature of the motor (Fig. 8). This network was inspired by the selected motor topology and includes both thermal resistances and capacities, so as to capture the motor thermal dynamics:

$$R = \frac{l}{\kappa A_\perp} \qquad C = \rho V c \tag{8}$$

Where l is the thickness of the material, κ is the thermal conductivity, $A_\perp$ is the area crossed by the heat flow, ρ is the material density, V is the volume and c the specific heat. The thermal power generators were instead computed considering the main loss mechanisms: Joule, hysteresis and eddy currents [14].

If the genetic optimization was aimed at the maximization of the electromagnetic torque, the thermal modelling was essential to verify the endurance of the performance. Since the motor is ventilated by the rotor, special care was taken in the modelling of the heat-transfer by convection, as a function of the induced air speed:

$$\dot{Q}_{ext} = \alpha_{ext} A_{case} \Theta_{case} \tag{9}$$

Where α_{ext} is the external convection coefficient, A_{case} is the external case surface and Θ_{case} is the temperature of the case with respect to the outside air, according to the helicopter altitude [15].

About convection. Four empirical models of forced convection for a flat plate were investigated in [16]. They differ from one another because of the hypotheses made about the flow (laminar or turbulent) and the surface

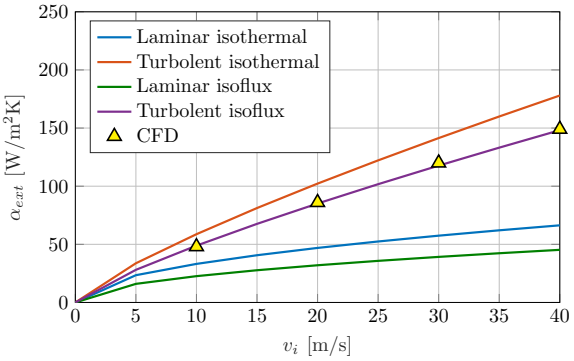

Figure 9: Convection coefficient correlations.

(isotherm or isoflux). The outcome of this study is reported in Fig. 9, where the convection coefficient correlations are plotted at sea level, for increasing values of the induced air speed. In order to decide which model worked better, a reduced CFD batch-simulation was set up and the relevant solution overlaid, suggesting to adopt the turbulent-isoflux combination.

3.3 Generator model

In order to deliver a useful anti-torque effect, tail motors require both a minimum level of power and voltage supply, which is closely related to the maximum achievable speed (or *base speed*). Fig. 3 shows a sketch of the electrical power generation and distribution network where, for sake of clarity, the several tail motors are fed by a single generator, through a single DC-bus, via simple three-phase inverters. The generator is also connected to the turbine output shaft (without gearbox) and rectified by a passive diode-bridge (without converter) because this solution would minimize the number of system parts and leverage the existing engine speed governor. Then, assuming for conservative reasons that the battery is not involved, the generator must be sized to provide the total power absorbed by the motors in the most demanding flight condition (HOGE). Note that the behavior of the generator is described by the same differential equations of the motors, in d-q. However, the inputs and the outputs are swapped and thermal modelling is omitted (since the generator could rely on a more effective liquid-cooling).

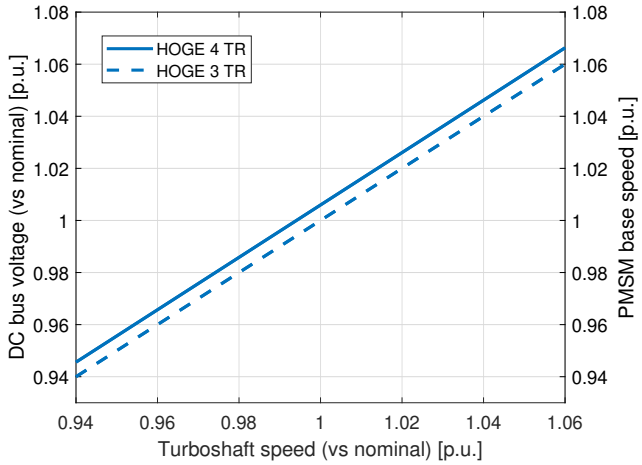

Figure 10: Thrust sensitivity to electrical generation.

With this model it has been possible to evaluate: how the DC voltage changes with respect to the turbo-shaft input speed; what is the impact of the load current on it (depending on the number of the active rotors); how the motor base speed (hence maximum thrust) is affected by the voltage droop. The outcome of this analysis is condensed in Fig. 10, which shows the margin to be taken in the generator design process, to ensure the full controllability of the aircraft in every flight condition.

3.4 Battery model

The reference battery technology is the Lithium-Ion (Li-ion). The interest in this chemistry has soared over the last decade due to its high energy density, high voltage and long operational life [17]. Nevertheless, it should be noted that high energy Li-ion cells contain additional chemicals which make them less stable and call for more sophisticated Battery Management Systems (BMS). This technology is also (currently) more expensive than any other, for the same capacity. A vast spectrum of battery models have been developed with varying degrees of physical insight, complexity and accuracy. They are typically classified as white, gray, and black box approaches [18]. The equivalent circuit models are part of the gray box models and they represent a good compromise between computational complexity and fidelity. Several equivalent circuit models are listed in the literature [19], and two approaches have been chosen from among them, according to the data available for the cells: the Thevenin, Fig. 11, and the Enhanced Self-Correcting (ESC) model [20].

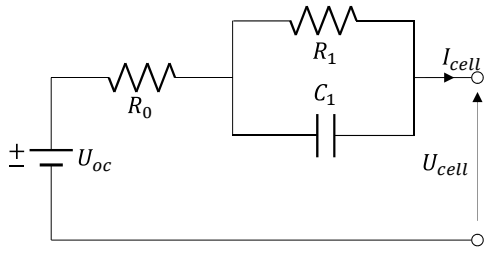

Figure 11: Thevenin cell model.

According to the proposed architecture, in case of complete engine failure (hence electrical generation loss), the system is supplied by an auxiliary battery pack. Therefore, this latter must be sized to deliver the power absorbed by the rotors, for the entire duration of the autorotation. This emergency maneuver sets a minimum power requirement (at the lowest SoC) and a minimum energy requirement (to complete the landing). In terms of the total number of cells N_{tot}:

$$N_{tot,E} \geq \frac{P_{pack}\,\Delta t}{Q_{cell}\,U_{cell}} \tag{10}$$

$$N_{tot,P} \geq \frac{P_{pack}}{I_{cell}\,U_{cell,min}} \tag{11}$$

Where, Q_{cell} is the real cell capacity (which differs from the nominal, depending on the actual discharge current I_{cell}), U_{cell} is the cell voltage and P_{pack} is the power released by the battery (supposed constant, during a discharge of Δt seconds). In order to satisfy both conditions, the maximum of the two solutions must be considered. Although there is not an established relationship, it can be tentatively assumed that $N_{tot,E}$ increases linearly by I_{cell} [21] and that for a certain discharge current, the total number of cells has a minimum (*sweet-spot*). This minimum is reached for $N_{tot,E} = N_{tot,P}$ which corresponds to the optimal discharge current, $I_{cell,opt}$. The optimal discharge current is thus a function of the cell capacity, the average voltage, the minimum voltage and total discharge duration:

$$I_{cell,opt} = \frac{Q_{cell}\,U_{cell}}{\Delta t\,U_{cell,min}} \tag{12}$$

In general, this is the target discharge current but it may happen that the maximum current not-to-exceed (e.g. for thermal/self-damaging reasons) is lower than the former and such to represent the effective discharge limit.

It can be also observed that $I_{cell,opt}$ in conjunction with equation (10) or (11) provides the minimum number of cells to build the pack, regardless of its topology. In order to define this battery pack topology, the following relationships must be introduced:

$$N_s = \frac{U_{pack}}{U_{cell,min}} \tag{13}$$

$$N_p = \frac{P_{pack}}{U_{pack}\, I_{cell}} \tag{14}$$

$$N_{tot} = N_s\, N_p \tag{15}$$

Where U_{pack} is the battery pack output voltage, N_p is the number of cells in parallel and N_s is the number of cells in series. For a given battery pack output voltage U_{pack}, it is thus possible to compute the number of cells in series and in parallel, which must be integer. Actually, this a further *hidden* condition which makes the total number of cells to increase by the number of cells in series, until a new parallel is formed. Therefore, it can happen that a better solution (such to minimize the total number of cells) is achieved accepting some degree of *flexibility* on the output voltage. In Fig. 12 is depicted the sizing process applied to commercially available battery cells. In particular, looking at Fig. 12a it is possible to notice that at the optimal discharge current the energy and the power sizing conditions converge. Looking at Fig. 12b it is instead possible to appreciate the fluctuation of the total number of cells and how it can be minimized only for certain pack topologies.

About the Battery Management System (BMS). This is a hardware and software component that regulates the correct operation and energy supply of the battery pack, protecting both the load and the source from abnormal conditions. In order to obtain a more realistic simulation of the system behavior, a simple logic based on the main system component information was developed and implemented. The BMS monitors the power that is required by the load and verifies if this is compatible with the generator capabilities (both in terms of current and voltage output). If these are adequate, the BMS tries to recharge the battery to keep its SoC in the optimal range (0.9 <SoC< 0.95). Otherwise, the battery is inserted and used to supply the motors (or to absorb the power that is regenerated, during active rotor braking).

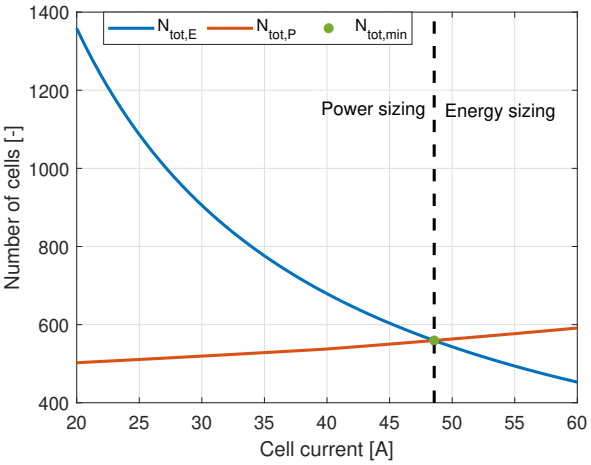

(a) Minimum cell number (target).

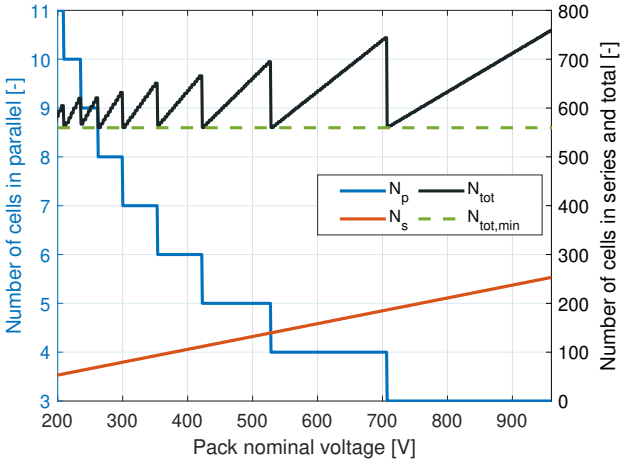

(b) Battery pack topology optimization.

Figure 12: Battery pack sizing.

4 SIMULATION RESULTS

The results of this section are relevant to the behavior of the anti-torque system, simulated for different test scenarios, using the models previously introduced. These models have been connected to form one single dynamic network and analyzed over three main physical domains: mechanical, thermal and electrical.

4.1 Rotor response

Fixed-pitch/variable-speed rotors are attractive for the inherent cost-effectiveness, and especially in the case of highly distributed propulsion systems. However, one of the major concerns regarding their use is about the achievable thrust response. Which is directly related to the angular speed response, governed by the torque balance equation at the rotor shaft:

$$J_{tr}\frac{d\omega_{tr}}{dt} = \tau_{em} - \tau_{tr}(\omega_{tr}) \tag{16}$$

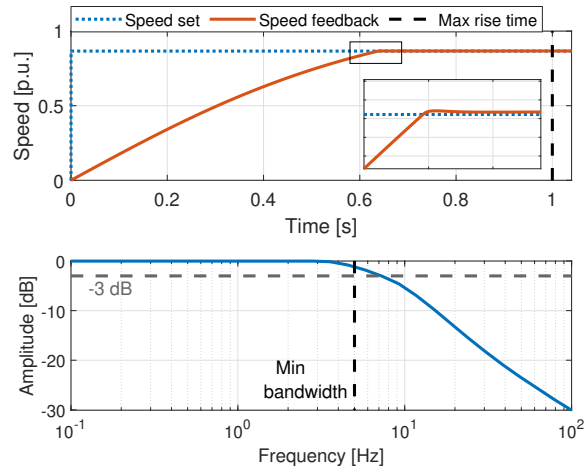

(a) Step response and Bode plot in HOGE (4 TR).

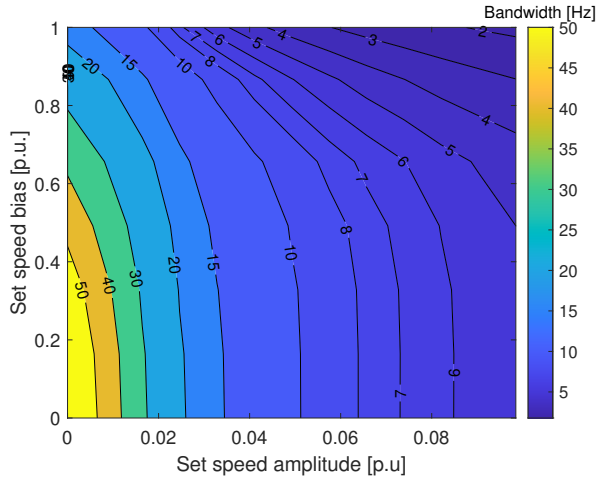

(b) Bandwidth cintours vs set amplitude and bias.

Figure 13: Rotor dynamics, simulation results.

Where J_{tr} is the inertia of the rotor assembly and τ_{em} is the electromagnetic torque produced by the motor.

Therefore, after that the electrical machine was optimized for steady operation, the angular speed response of each rotor/motor unit was verified integrating Eq. (16) as part of the adopted motor control scheme, and tuning the relative control gains. The resulting behavior was then analyzed and compared against the minimum acceptance criteria. Note that the angular speed acceptance criteria are not immediately available but can be derived from the legacy helicopter requirements. Which are usually expressed in terms of the displacement of the servo-hydraulic actuator, controlling the pitch angle of the blades [22].

In particular, the time-response should be equivalent to a full stroke in one second, and the frequency-bandwidth equal/better than 5 Hz, for a command amplitude of $\pm 10\%$ at the maximum rotor thrust. While the former directly compares with a *full speed* in one second, the latter can be translated using Eq. (4) and recalling the fact that thrust is linearly proportional to the angle of attack (within the blade stall limits). So that for the same thrust effect, a pitch amplitude of $\pm 10\%$ corresponds to a rotor speed amplitude of $\pm 5\%$, at the maximum bias.

Fig. 13 summarizes the results of the rotor response simulation. More in detail, Fig. 13a shows the time response to a step signal equal to the speed in HOGE (with 4 TR) along with the frequency response for a signal amplitude equal to $\pm 5\%$ of the same bias. This proves that the thrust response is comparable with that of a legacy pitch controlled system [23]. However, the thrust bandwidth tends to shrink by the rotor speed, which is a distinguishing feature of non-linear systems [24]. This is evident looking at Fig. 13b which shows a map of the bandwidth for different combinations of the set amplitude and the bias. Such contraction should be carefully considered in case of side wind (hence abnormal rotor speed) since the thrust response may become critical for the aircraft controllability.

4.2 Motor endurance

While the previous analysis focused on the rotor response, the following intended to verify the motor capability to sustain the required load for the minimum duration associated with each flight condition. Even in the presence of two failures, so that a pilot can abort the mission and return safely to the base.

As already observed, from this perspective, the worst scenario corresponds to the loss of one motor unit in HOGE. In which case, the total disc area would shrink to 3/4 of the original. Requiring more torque, at a higher angular speed, hence much more power to control the aircraft. So that the maximum heating and the maximum over temperature are produced. The results of a mission simulation affected by a motor/rotor loss are reported below. More in details, Fig. 14a shows the mean value of the motor speed reference (or *bias*), through the helicopter take-off (1 minute), climb (5 minute), cruise (11 minute) and HOGE (4 minute). At this point, one of the tail motors fails, forcing the others near their power peak.

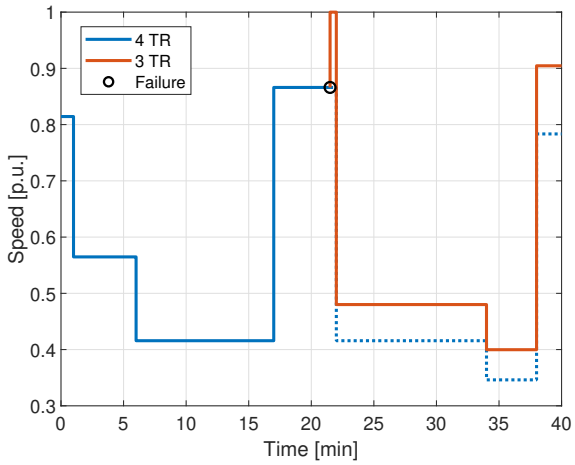

(a) Motor speed reference: from 4 TR to 3 TR.

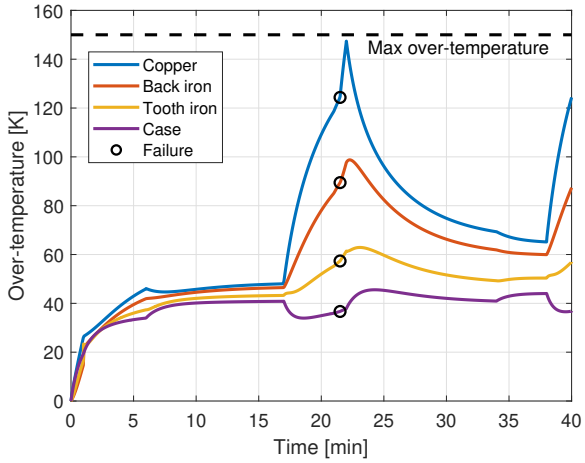

(b) Motor temperature rise, from 4 TR to 3 TR.

Figure 14: Mission simulation with 1 TR loss (in HOGE)

After 30 seconds of HOGE in this condition, the pilot returns to the base through an additional cruise (12 minutes), descent (4 minutes) and vertical landing (2 minutes). Consistently, Fig. 14b shows the thermal behavior of the motor through the same mission profile. From which it is possible to appreciate that the temperature peak is reached by copper (i.e. the motor winding), with an overshoot of +20 K upon the failure, still below the 150 K limit of the insulators. This proves that the proposed concept has an intrinsic redundancy degree and that it can provide a residual capability useful to complete (or abort safely) a mission. Even in the case of a complete rotor/motor loss, after which the system would absorb approximately +15% power (+50% per unit).

4.3 Battery discharge

Helicopter engines are normally connected to the drive train through a freewheel device, which in case of failure, automatically disengages the output shaft and allows the pilot to land safely, in *free* main rotor autorotation. During this phase, the mechanical link between the main and the tail rotor drives the latter and ensures that the pilot can control the yaw of the aircraft [12]. In the proposed electrical architecture, the mechanical link is instead absent and since the generator is supposed integrated with the engine, an auxiliary battery is needed to supply the tail motors (ref. to Sec. 3.4). Assuming that the failure occurs at the maximum ceiling, it has been verified by simulation what would be the system behavior, over a period of approximately 10 minutes, while running on battery.

The results of the battery discharge are presented in Fig. 15, where the most interesting part is the *entry* in autorotation. During this transient of just 6 seconds, the battery takes over the generator, tail rotors slow down and thrust is inverted. Thrust inversion is facilitated by the motor active braking, which in return regenerates a negative current (hence power). The rotors are then accelerated again towards a new negative speed set point, associated with a new positive power level (Fig. 15a). This level is then held for the rest of descent, until the final flare and the helicopter touch-down. As shown in Fig. 15b, the current of the cells remains always within the manufacturer specification, while the battery voltage droop is limited to approximately 40%. Which ensures that the battery can provide the required power, for the entire duration of the descent, plus a certain margin for the final stages.

5 CONCLUSION

The behaviour of a distributed electric anti-torque system concept for single main rotor helicopters has been preliminary investigated using a multi-physics modelling and simulation approach. The authors started from an assigned usage spectrum and rotor design; introduced the reference electrical technology; discussed the system architecture in connection with the safety requirements; recalled the equations expressing the capability of each main component; described a preliminary optimization of the involved motor and battery units; presented the results of the system simulation with respect to a number of testing scenarios. The concept proposed in this paper has thus demonstrated the following, distinctive advantages and disadvantages.

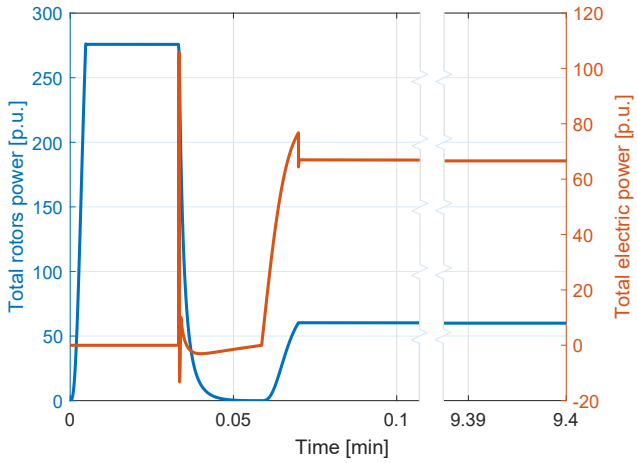

(a) Rotor vs motor (total) absorbed power.

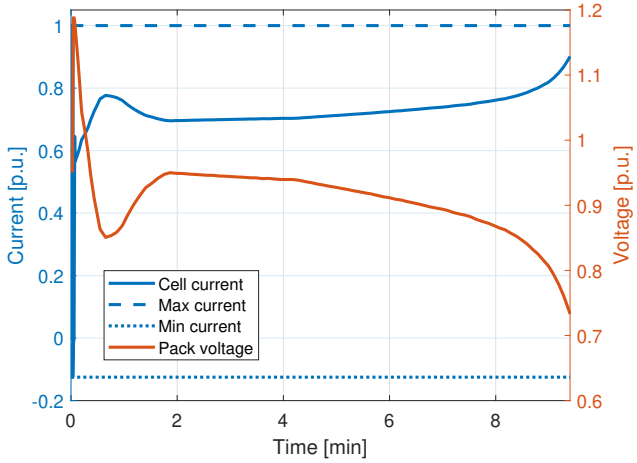

(b) Cell current and battery pack voltage.

Figure 15: Autorotation simulation (from max. ceiling).

Advantages:

1. Simplification of the tail rotor design into a *fan*, still offering a thrust response comparable to that of a traditional pitch controlled system.

2. Soft-fail or *graceful degradation* of the anti-torque functionality, ensuring the vertical landing capability by contrast to a single rotor point of failure.

3. Reduced total motor weight, as a consequence of the direct dependency of the electrical machines mass on torque (not power).

Disadvantages:

1. Should a motor fail, the equivalent total disc loading is increased and the system efficiency is reduced.

2. For a given rotor/motor design, the system bandwidth tends to shrink by the angular speed, which may be critical in case of side wind.

3. Generation backup on battery is only feasible for very short periods of time, also due to the voltage droop limiting the tail motor base speed.

Notably, the use of DEP could save approximately 30% of the motor active weight, compared to an equivalent concentrated solution [4], while the weight of a battery pack optimized for emergency landing should be similar to that of the system generator. Under these assumptions, at the current state-of-the-art, the penalty due to the electrification of the anti-torque system may be stated at $1 \div 2\%$ of a typical medium class helicopter Maximum Take Off Weight (MTOW). This may be considered the price to pay for an increased safety and a reduced maintenance, but a proper evaluation of the system potential should be formulated in the framework of a *more-electric helicopter*. For which the design and development of this and other electrical systems could be optimized by synergy, from the beginning.

The incubation of the present solution at a higher Technology Readiness Level (TRL) is now expected to pass through a test session on dynamometer (to verify the motor fault tolerance), in wind tunnel (to verify the rotor thrust superposition) and on flight simulator (to verify the aircraft controllability, with pilot-in-the-loop).

ACKNOWLEDGEMENTS

This research is dedicated to *Paul Brinson* and his evolutionary vision of a future helicopter that can achieve new standards of flexibility, reliability and efficiency through a more powerful and integrated electrical network.

REFERENCES

[1] H. D. Kim, A. T. Perry, and P. J. Ansell, "A review of distributed electric propulsion concepts for air vehicle technology," in *2018 AIAA/IEEE Electric Aircraft Technologies Symposium*. DOI: 10.2514/6.2018-4998.

[2] F. D. Harris, E. F. Kasper, and L. E. Iseler, "U.s. civil rotorcraft accidents, 1963 through 1997," NTRS-NASA Technical Memorandum, Tech. Rep., 2000.

[3] P. Mellor, J. Yon, S. Williamson, *et al.*, "Electrical machine technologies for an electric tail rotor drive," in *European Rotorcraft Forum*, 2015.

[4] K. Stickels, M. Brunetti, M. Barber, *et al.*, "Advances in helicopter electric tail rotor drive," in *European Rotorcraft Forum*, 2017.

[5] A. Datta, "Electric-vtol research at university of maryland - simulation, design, and flight testing," in *Electric and Hybrid Aerospace Technology Symposium (EHATS)*, 2017.

[6] F. Salomez, S. Vienot, B. Zaidi, *et al.*, "Design of an integrated gan inverter into a multiphase pmsm," in *2020 IEEE Vehicle Power and Propulsion Conference (VPPC)*, 2020, pp. 1–6. DOI: 10.1109/VPPC49601.2020.9330956.

[7] Federal Aviation Administration (FAA), Advisory Circular 29-2C, *Certification of Transport Category Rotorcraft, (Changes 1-8 incorporated)*. U.S. department of transportation, September 30, 2008.

[8] D. Michieletto, N. Bianchi, and M. Brunetti, "Dual three-phase motor fault tolerance for modern transport," in *2021 International Aegean Conference on Electrical Machines and Power Electronics (ACEMP), and 2021 International Conference on Optimization of Electrical and Electronic Equipment (OPTIM)*, 2021, pp. 405–412. DOI: 10.1109/OPTIM-ACEMP50812.2021.9590040.

[9] M. A. Rendón, C. D. Sánchez R., J. Gallo M., and A. H. Anzai, "Aircraft hybrid-electric propulsion: Development trends, challenges and opportunities," *Journal of Control, Automation and Electrical Systems*, pp. 1–25, Jun. 2021. DOI: 10.1007/s40313-021-00740-x.

[10] J. M. Seddon, "An account of first principles in the fluid mechanics and flight dynamics of the single rotor helicopter," in *Basic Helicopter Aerodynamics*, 1990. DOI: ISBN0-632-02032-6.

[11] K. C. Kim, "Analytical calculations of helicopter torque coefficient and thrust coefficient values for the helicopter performance (helpe) model," in *US Army Research Laboratory ARL-TR-1986*, 1999.

[12] W. Johnson, *Helicopter Theory*, First. Dover Publications, 1994, ISBN: 9780486682303.

[13] N. Bianchi, D. Michieletto, L. Cinti, *et al.*, "Permanent magnet synchronous motor drives for more-electric aircraft," in *Symposium on Power Electronics, Electrical Drives, Automation and Motion (SPEEDAM)*, 2022.

[14] I. Boldea and L. N. Tutelea, *Electric Machines: Transients, Control Principles, Finite Element Analysis, and Optimal Design with MATLAB®*, Second. CRC Press, Taylor & Francis Group, 2022.

[15] ISO 2533:1975, *Standard Atmosphere*. Geneva, CH: International Organization for Standardization, May 1975.

[16] P. S. Ghahfarokhi, A. Kallaste, A. Belahcen, and T. Vaimann, "Determination of heat transfer coefficient for the air forced cooling over a flat side of coil," *Electrical, Control and Communication Engineering*, vol. 15, no. 1, pp. 15–20, 2019. DOI: doi:10.2478/ecce-2019-0003.

[17] T. B. Reddy, *Linden's Handbook of Batteries*, Fourth. McGraw-Hill Education, 2011, ISBN: 9780071624190.

[18] S. Tamilselvi, S. Gunasundari, N. Karuppiah, *et al.*, "A review on battery modelling techniques," *Sustainability*, vol. 13, no. 18, 2021, ISSN: 2071-1050. DOI: 10.3390/su131810042.

[19] H. He, R. Xiong, and J. Fan, "Evaluation of lithium-ion battery equivalent circuit models for state of charge estimation by an experimental approach," *Energies*, vol. 4, no. 4, pp. 582–598, 2011, ISSN: 1996-1073. DOI: 10.3390/en4040582.

[20] G. L. Plett, *Battery Management Systems*, Second. Artech House, 2020, ISBN: 9781630810276.

[21] C.-k. Chang, "Factors affecting capacity design of lithium-ion stationary batteries," *Batteries*, vol. 5, no. 3, 2019, ISSN: 2313-0105. DOI: 10.3390/batteries5030058.

[22] A. Nesci, A. De Martin, G. Jacazio, and M. Sorli, "Detection and prognosis of propagating faults in flight control actuators for helicopters," *Aerospace*, vol. 7, no. 3, 2020, ISSN: 2226-4310. DOI: 10.3390/aerospace7030020.

[23] A. De Martin, G. Jacazio, A. Nesci, and M. Sorli, "In-depth feature selection for phm system's feasibility study for helicopters' main and tail rotor actuators," in *PHM Society European Conference*, vol. 5, 2020, p. 9. DOI: 10.36001/phme.2020.v5i1.1222.

[24] A. C. Bertolino, A. De Martin, A. Nesci, and M. Sorli, *Meccatronica: analisi progettazione e modellazione di servosistemi*. Torino, Italy: CLUT, 2021.